Enhanced Enzymatic Activity through Photoreversible Conformational Changes†

Shao-Chun Wang and C. Ted Lee, Jr.*

Department of Chemical Engineering and Materials Science, University of Southern California, Los Angeles, California 90089-1211

Received June 1, 2007; Revised Manuscript Received October 2, 2007

ABSTRACT: The interaction of a light-responsive surfactant with lysozyme at pH 5.0 has been investigated as a means to control protein structure and enzymatic activity with light illumination. The cationic azobenzene surfactant undergoes a reversible photoisomerization upon exposure to the appropriate wavelength of light, with the visible-light (*trans*) form being more hydrophobic and, thus, inducing a greater degree of protein unfolding than the UV-light (*cis*) form. Conformational changes as a function of photoresponsive surfactant concentration and light illumination were measured through shape-reconstruction analysis of small-angle neutron scattering (SANS) data. The SANS-based *in vitro* structures indicate that lysozyme transitions from a nativelike structure at low surfactant concentration to a partially unfolded conformation at higher surfactant concentrations under visible light illumination, while UV-light illumination causes the protein to refold to a near-native structure. Protein swelling occurs principally away from the active site near the hinge region connecting the α and β domains, leading to an increase in the observed separation distance of the α and β domains in the ensemble SANS measurements, a likely result of enhanced domain motions and increased flexibility within the protein. This swelling of the hinge region is accompanied by an 8-fold increase in enzymatic activity relative to the native state. Both enzyme swelling and superactivity observed under visible light can be reversed to nativelike conditions upon exposure to UV light, leading to complete photoreversible control of the structure and function of lysozyme.

Azobenzene-based photoresponsive surfactants have recently been utilized to induce reversible changes in protein conformation with light illumination, with relatively high resolution *in vitro* protein structures during the structural transitions determined with small-angle neutron scattering (SANS[1]) (*1*−*4*). A photoisomerization between the *trans* (relatively hydrophobic) and *cis* (relatively hydrophilic) forms of the azobenezene moiety allows photocontrol of a wide range of surfactant properties (*5*), including interaction with various protein domains. For bovine serum albumin (BSA) in the presence of the photosurfactant, the initial unfolding events were localized to the hydrophobic α-helical segments in the C-terminal portion of the protein (*1*, *3*). Furthermore, through changes in light illumination, reversible transitions between intermediately folded conformations were achieved. In contrast, for α-chymotrypsin with a primarily β structure, only small changes in the overall size of the protein were observed (∼7% increase in the radius of gyration), however, this subtle structural rearrangement was sufficient to convert *intramolecular* β structures into *intermolecular* β sheets and lead to eventual amyloid fibril formation. From the pre-amyloid oligomer structures determined with SANS, photoreversible transitions from corkscrewlike hexamers to ropelike dodecamers were observed, potentially capturing the initial stages of fibril formation. For lysozyme containing both α and β domains, SANS data indicated that the photosurfactant primarily swelled the α-domain of the protein and particularly helix A, while the β-domain and the active-site cleft remained relatively intact (*2*). From these structural studies in lysozyme, the question remains as to what effect, if any, would the reversible changes in protein conformation have on enzymatic activity.

Protein function is, to a large extent, determined by protein conformation, particularly in the case of enzymes where folding results in an active site that allows for selective binding of substrates. However, the static form−function relationship of the classic "lock-and-key" mechanism has been replaced in modern enzymology with the view that enzyme dynamics can have an equally important role in catalysis. Thus, various hypotheses have been proposed with this view in mind (*6*−*10*), all with the underlying theme that significant conformational flexibility is required during the course of the reaction (*11*). Thus, it is generally viewed that for the enzyme−substrate complex to surpass the activation-energy barrier requires "conformational sampling" (*8*) or "dynamic excursions" (*12*) along the reaction pathway toward the formation of transition-state conformations (*13*, *14*). Interestingly, this flexibility is not necessarily proximal to the active site, and instead may be in distal regions away from the active site (*8*, *15*, *16*). This has been demonstrated

† This material is based upon work supported by the National Science Foundation under Grant No. 0554115.

* Author to whom correspondence should be addressed. Phone: (213)740-2066. Fax: (213)740-8053. E-mail: shaochuw@usc.edu and tedlee@usc.edu.

[1] Abbreviations: SANS, small-angle neutron scattering; BSA, bovine serum albumin; azoTAB, azobenzene trimethylammonium bromide; Ml-RBB, *Micrococcus luteus* conjugated with Remazol brilliant blue; RBB-R, Remazol brilliant blue R; glycolchitin-RBB, glycolchitin conjugated with Remazol brilliant blue; PDDFs, pair distance distribution functions; SDS, sodium dodecyl sulfate.

10.1021/bi701073d CCC: $37.00
Published on Web 11/22/2007

through various mutation studies where replacement of distal amino acids has led to concurrent changes in reaction rates and protein flexibility, potentially by increasing the probability of sampling transition-state conformations (*15*, *17*). These results seem to suggest a general procedure by which enzymatic activity could be increased through enhancements in enzyme flexibility, provided that these enhancements are not achieved at the expense of denaturing the active site.

Lysozyme catalyzes the hydrolysis of $\beta(1\rightarrow4)$ linked polysaccharide copolymers of *N*-acetylglucosamine and *N*-acetylmuramic acid found in certain bacteria cell walls, as well as homopolymers of *N*-acetylglucosamine (i.e., chitin). The enzyme active site, divided into 6 subsites *A* through *F*, resides in a cleft between the two domains of lysozyme: the α-domain folded around a central hydrophobic core containing four α-helices and one 3_{10} helix, and a sheet-like β-domain consisting mainly of hydrophilic residues either on the outer surface of the molecule or lining the cleft. The cleavage of $\beta(1\rightarrow4)$ linkages occurs between sites *D* and *E* close to the catalytic residues Glu35 and Asp52 (*18*), leading to formation of an oxocarbenium intermediate that is electrostatically stabilized by Asp52. This intermediate can then be hydrolyzed upon direct attack by a nucleophilic water molecule (hydrolysis) completing the reaction, or a $\beta(1\rightarrow4)$ linkage can be regenerated upon reaction with a second substrate molecule that becomes bound to the vacant subsites *E* and *F* (transglycolsylation) (*19*−*21*).

Enhanced lysozyme activity has been observed upon modification of specific amino acids within the protein. For example, a mutant lysozyme with deleted Arg14 and His15 residues (both located in helix A of the α domain distal to the active site) was observed to exhibit increased activity (∼140%) attributed to enhanced mobility of the residues near or at the active site (*22*, *23*). Conversely, the presence of ionic surfactants such as sodium *n*-alkyl sulfates and *n*-alkyl trimethylammonium bromides usually deactivates the enzyme by interacting directly with the active site or indiscriminately denaturing the protein (*24*−*27*). These alkyl-based surfactants unfold all regions of the protein through nonspecific interactions with protein hydrophobic domains. In contrast, the "localized swelling" of lysozyme observed in the presence of the azobenzene-based photosurfactant in regions away from the active site suggests that the effect of the photosurfactant on lysozyme activity could be unique from traditional surfactants, potentially increasing reactivity through enhancements in protein flexibility.

In the present work, the conformation and activity of lysozyme are controlled through the use of a photoresponsive surfactant and light illumination. Shape-reconstruction analysis (*28*, *29*) of small-angle neutron scattering data is used to provide relatively high-resolution information on the location of protein unfolding. The observed conformational changes are correlated with enzyme activity measured through two different assays, *Micrococcus Luteus* and glycolchitin. The photosurfactant is found to swell the hinge region connecting the α and β domains, leading to a more flexible protein and resulting in dramatic increases in enzyme activity. Moreover, the observed light-induced superactivity can be photoreversibly controlled through surfactant isomerization.

EXPERIMENTAL PROCEDURES

An azobenzene trimethylammonium bromide surfactant (azoTAB) of the form

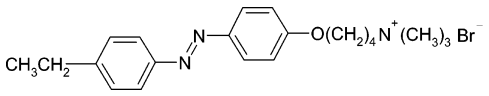

was synthesized according to published procedures (*30*, *31*). The surfactant undergoes a reversible photoisomerization upon exposure to the appropriate wavelength of light with the *trans* isomer (434-nm visible light) exhibiting a lower dipole moment and, hence, being more hydrophobic than the *cis* isomer (350-nm UV light) (*30*).

To eliminate the potential of UV deactivation of the enzyme (*32*−*34*), *cis* surfactant solutions were preconverted under UV-light from an 84-W long wave UV lamp, 365 nm (Spectroline, model number XX-15A) for at least 30 min prior to the addition of an enzyme stock solution. The combined solutions were then maintained in the dark during the entire reaction period of 1−3 h, with absorbance spectra measured after each experiment to ensure the surfactant remained in the *cis* form (the half-life of dark conversion from the *cis* to the *trans* form is ∼24 h) (*35*). However, control experiments demonstrated that activity was unaffected by direct UV illumination of the enzyme in the presence of the photosurfactant. Thus, azoTAB appears to offer similar protective properties as other UV scavengers such as ascorbate (*32*, *33*) due to the strong absorbance of the surfactant in the UV region. In contrast, pure enzyme showed an ∼70% decrease in activity upon exposure to UV light.

For the dynamic photoresponse assays and optical microscopy, conversion to the *cis* form was achieved by illuminating the enzyme−surfactant solutions with a liquid light guide (Oriel, model number 77557) attached to a 200-W mercury arc lamp (Oriel, model no. 6283) equipped with a 320-nm band-pass filter (Oriel, model no. 59800) in combination with a heat-absorbing filter (Oriel, model no. 59060), effectively isolating the 365-nm mercury line (UV-A). Conversion back to the *trans* form was achieved with a 400-nm long-pass filter (Oriel, model no. 59472) to isolate the 436-nm mercury line.

Enzymatic Assays

Highly purified lysozyme from hen egg white (L7651), lyophilized *Micrococcus luteus* (M3770), glycolchitosan (G7753), Remazol brilliant blue R (R8001) and phosphate buffer (8.3 mM) were purchased from Sigma and used as received. The buffer was adjusted to pH 5.0 with the addition of HCl. The standard lysozyme assay of monitoring the decrease in optical density during lysis of *Micrococcus leteus* cells walls was deemed inappropriate in the presence of azoTAB due to potential surfactant-induced cell aggregation (see below). Hence, the alternative assays described below were utilized.

Preparation of Micrococcus luteus Conjugated with Remazol Brilliant Blue (Ml-RBB). Ml-RBB was prepared as described by Ito et al. (*36*) To 40 mL of a suspension of *Micrococcus luteus* cells (15 mg/mL), a solution of 400 mg of Remazol brilliant blue R (RBB-R) in 40 mL of distilled water was slowly added under constant stirring at 50 °C.

Subsequently, 8 g of sodium sulfate was added over the course of 30 min. A solution of 400 mg of trisodium phosphate in 4 mL of distilled water was then added, and the mixture was stirred at 50 °C for another 30 min. The mixture was centrifuged at 2600 rpm for 10 min, and the supernatant was discarded. The pellet was washed with 40 mL of phosphate buffer (50 mM) until the supernatant was colorless, followed by washing twice with distilled water. Ml-RBB was then lyophilized and stored at −20 °C.

Preparation of Glycolchitin Conjugated with Remazol Brilliant Blue (Glycolchitin-RBB). Glycolchitin-RBB was obtained by acetylation of glycolchitosan (*37*) followed by coloration with RBB-R (*38*, *39*). Briefly, 1.5 g of glycolchitosan, a water-soluble derivative of chitosan, was dissolved in 150 mL of sodium tetraborate solution (100 mM). Acetic anhydride was then slowly added under constant stirring until an acetic acid concentration of 2 wt % was reached, followed by adjusting to pH 9 with NaOH. After 30 min, glycolchitin was precipitated from the mixture by addition of acetonitrile, repeated several times until the pH of the glycolchitin solution was neutral. The product obtained was then dissolved in 75 mL of water and gently heated to 50 °C, with a RBB-R solution (150 mg/mL) slowly added under constant stirring. After an hour, 3 g of sodium sulfate was added in several aliquots, with 0.3 g of trisodium phosphate subsequently added with the reaction continued for another 75 min at 50 °C. Glycolchitin-RBB was then dialyzed against water for 2 days to remove excess dye, salts, and low molecular weight product. The final product was lyophilized and stored at −20 °C.

Lysozyme Activity against Ml-RBB. 1.6 mg/mL of Ml-RBB was suspended in an 8.3 mM, pH 5.02 phosphate buffer. A 1.0 mL lysozyme solution (0.008 mg/mL), 1.0 mL buffer solution, and the desired amount of a stock surfactant solution were then added to 2.0 mL of the Ml-RBB suspension. The reaction mixture was then incubated at 37 °C with continuous, gentle stirring. At suitable time intervals, 400 μL of the reaction volume was withdrawn and immediately vortexed for 10 s to quench the reaction due to unfolding of the enzyme induced by exposure to the air−liquid interface (*40*, *41*), followed by centrifugation at 15,000 rpm for 5 min to remove the insoluble cell walls, leaving the hydrolyzed reaction product remaining in the supernatant. The absorbance of the supernatant at 600 nm was measured and found to increase linearly with time for 2 h. Lysozyme activity at different conditions was determined from the initial rate of increase of the absorbance at 600 nm due to the dyed product, expressed as a percentage relative to pure lysozyme. Activity of a lysozyme solution was measured after vortexing the enzyme solution for 10 s confirming loss of activity due to unfolding.

Lysozyme Activity against Glycolchitin-RBB. 1 mL of glycolchitin-RBB (2 mg/mL) was mixed with 0.5 mL of an azoTAB solution at appropriate concentrations and 0.5 mL of a lysozyme solution (0.008 mg/mL) in an 8.3 mM, pH 5.02 phosphate buffer to give a final concentration of 1 mg/mL glycolchitin-RBB and 0.002 mg/mL lysozyme. The mixture was incubated at 37 °C under gentle stirring. At suitable time intervals 200 μL of the reaction volume was withdrawn and mixed with 200 μL of acetoniltrile to quench the reaction and precipitate nonreduced glycolchitin. The mixture was then cooled on ice and centrifuged at 15,000 rpm for 5 min at room temperature. Lysozyme activity was determined from the initial rate of increase of the absorbance at 600 nm over the range of 1 h, expressed relative to the rate of pure lysozyme.

Kinetic parameters of lysozyme with and without the presence of azoTAB were obtained using substrate concentrations ranging from 0.01 to 0.44 wt % of glycolchitin-RBB. The reaction mixture was incubated at 37 °C for 1 h. The maximum initial velocity V_m and the apparent Michaelis constant K_M of the enzyme were determined from linear-regression analysis of double-reciprocal Lineweaver−Burk plots. Data that demonstrated inhibition due to high substrate concentration and, thus, presented an upward trend in the Lineweaver−Burk plots were excluded from the analysis of kinetic parameters. According to the Lineweaver−Burk equation ($1/\upsilon = 1/V_m + K_M/V_m[S]$, where υ and [S] represent the initial velocity and substrate concentration, respectively), K_M was obtained from the *x*-axis intercept of $-1/K_M$, while V_m was determined from the *y*-axis intercept of $1/V_m$. Due to the inability to determine the accurate molecular concentration of the polymer substrate in the reaction mixture, V_m is presented as the change of absorbance at 600 nm per minute.

Optical Microscopy of ML-RBB Cells. 2.0 mL of a stock azoTAB surfactant solution was added to 2.0 mL of a 1.6 mg/mL Ml-RBB suspension in an 8.3 mM, pH 5.02 phosphate buffer. The samples were then observed with an Olympus IX71 inverted microscope equipped with a 40× objective lens (SLCplanFl) and a 1.6× magnification changer resulting in 64× total magnification, and recorded with a CCD digital camera (Hamamatsu, model no. C4742-95). At each azoTAB concentration, the same solution was used to obtain images under both visible and UV light with the samples exposed to UV light for at least 30 min to convert the surfactant to the *cis* form.

Small-Angle Neutron Scattering

The neutron scattering data were collected on the 30-m NG3 SANS instrument at NIST (*42*). Two sample−detector distances were used (1.33 and 7.0 m) combined with a 25-cm detector offset to give a *Q*-range of 0.0048−0.46 Å^{-1}, where $Q = 4\pi\lambda^{-1}\sin(\theta/2)$ and θ is the scattering angle. The net intensities were corrected for the background and empty cell (pure D_2O), followed by accounting for the detector efficiency using the scattering from an isotropic scatterer (Plexiglass), and then converted to an absolute differential cross section per unit sample volume (in units of cm^{-1}) using an attenuated empty beam. The coherent scattering intensities of the sample were obtained by subtracting the incoherent contribution from the hydrogen atoms in lysozyme (0.004 cm^{-1}) and the surfactant (0−0.0012 cm^{-1}).

The SANS data were analyzed using three complementary techniques: Guinier analysis, calculation of the pair distance distribution functions (PDDFs), and a shape-reconstruction algorithm. The PDDFs were calculated assuming a monodisperse system using GNOM (*28*) over a *Q*-range of ca. 0.02−0.3 Å^{-1} to exclude protein intermolecular interactions at low *Q* (*2*, *4*). The maximum particle diameter (D_{max}) was selected to give a smooth return of the PDDF to zero at D_{max}. The shape reconstructions were performed by approximating lysozyme as containing 1000 scattering centers in the

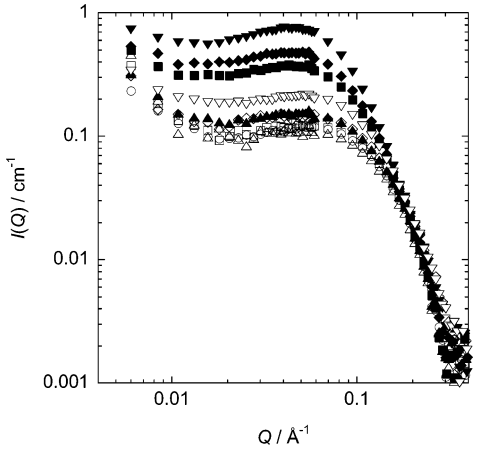

FIGURE 1: SANS data of lysozyme-azoTAB solutions as a function of surfactant concentration under visible (closed symbols) and UV (open symbols) light. Pure lysozyme (○), 3.6 mM azoTAB (▲, △), 8.5 mM azoTAB (■, □), 12.0 mM azoTAB (◆, ◇), and 18.6 mM azoTAB (▼, ▽). [Lysozyme] = 10 mg/mL in pH 5.0 buffer.

program GA_STRUCT (*29*) over a *Q*-range of 0.01−0.3 Å^{-1}, again to exclude intermolecular interactions and to avoid length scales too small for protein continuity at high *Q*. Briefly, GA_STRUCT utilizes a genetic algorithm to optimize the positions of the 1000 scattering centers until the calculated scattering data best fit the experimental data. Ten independent runs are performed, with the individual protein shapes from each run averaged to give the consensus envelope (*29*).

RESULTS AND DISCUSSION

The ability to control lysozyme conformation with azoTAB surfactant at pH 5.0 is shown in the SANS data in Figure 1 as a function of azoTAB concentration and light conditions. Under visible light at even the lowest azoTAB concentration studied (3.6 mM), the scattering curves begin to deviate from pure lysozyme at $Q \sim 0.2$ Å^{-1} or length scales ($L = 2\pi/Q$) of approximately 31 Å, similar to the diameter of lysozyme (36 Å) (*43*). This suggests that lysozyme swells with increasing *trans* azoTAB concentration. Under UV light, however, with the surfactant converted to the *cis* state, evidence of swelling is not observed until 12.0 mM azoTAB, or about 3−4 times the concentration under visible light. Thus, over a wide concentration region photoreversible protein folding can be achieved, similar to previous results obtained at pH 7 (*2*).

From the data in Figure 1, radii of gyration (R_g) were calculated from the Guinier approximation $I(Q) = I(0)\exp(-Q^2R_g^2/3)$, valid in the region $QR_g < 1.3$. As seen in Table 1, azoTAB under both visible and UV light increases the values of R_g relative to the pure lysozyme ($R_g = 12.9$ Å, in good agreement with published values of the native state of 13.3 and 13.5 Å (*2*, *44*)), with again the deviation from the native state greater under visible comparing to UV light. Note, however, that even the largest value of $R_g = 19.2$ Å in Table 1 is relatively low compared to values reported for denatured lysozyme in urea ($R_g = 28.7$ Å) and alcohol ($R_g = 24.9$ Å) (*45*), suggesting relative mild swelling of the protein with azoTAB.

Pair distance distribution functions (PDDFs) shown in Figure 2, related to the probability $P(r)$ of finding two

Table 1: Values of the Radius of Gyration Determined from Guinier Analysis of the SANS Data in Figure 1

[azoTAB] (mM)	R_g (Å)
0.0	12.9
Visible Light	
3.6	13.9
8.5	17.0
12.0	17.8
18.6	19.2
UV Light	
3.6	12.8
8.5	12.8
12.0	13.2
18.6	14.2

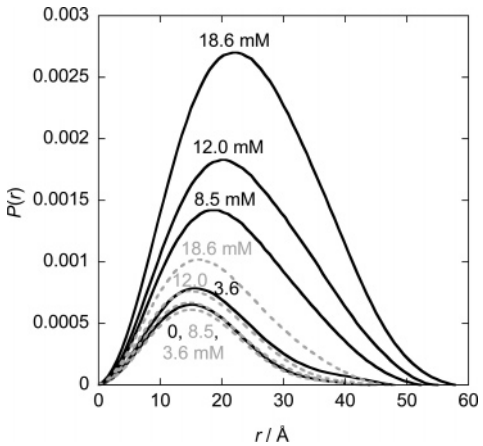

FIGURE 2: PDDFs of lysozyme-azoTAB solutions as a function of surfactant concentration under visible (solid, black lines) and UV (dashed, gray lines) light. [Lysozyme] = 10 mg/mL in pH 5.0 buffer.

scattering centers within the protein a distance *r* apart, were calculated from the SANS data in Figure 1. For a globular protein, the PDDF is expected to have a symmetric, inverse parabolic shape with a peak position and maximum dimension (D_{max}) approximately given by the protein radius and diameter, respectively. As seen in Figure 2, increasing azoTAB concentration under visible illumination results in D_{max} increasing from 42 Å to 57 Å, while the peak maxima shift from ∼15 Å to 22 Å. Under UV light less effect is again observed, consistent with a smaller degree of unfolding with the *cis* surfactant. For comparison, D_{max} increases from 42 Å to 75 Å in lysozyme denatured with urea (*46*).

To gain more precise information on the nature of protein unfolding with azoTAB, a shape-reconstruction algorithm was applied to the SANS data. As previously described (*2*), the protein is approximated as a collection of scattering centers whose positions are adjusted to fit the experimental scattering curve. The results of this shape reconstruction analysis are shown in Figure 3 along with the X-ray crystallographic structure of lysozyme (PDB code 6LYZ). The structures from the runs best fitting the data are shown in blue, while the "consensus envelopes" obtained by averaging the 10 independent runs for each data set are displayed in red to demonstrate consistency of the fits. Although the resolution of the SANS technique ($\sim 2\pi/Q_{max}$) (*28*) is reduced compared to X-ray crystallography, these and similar (*29*, *47*) structures have demonstrated the ability of SANS to determine precise structural detail of proteins *in vitro*, such as location of the active site cleft of lysozyme

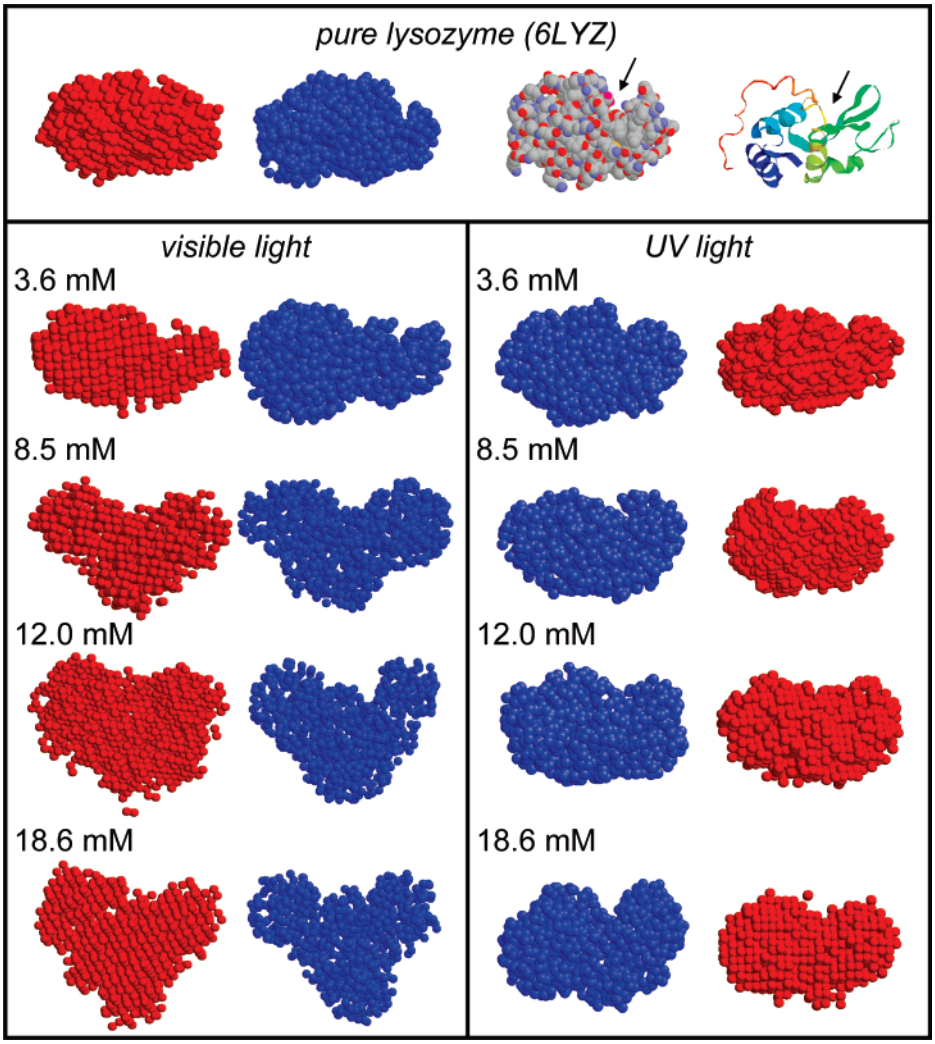

FIGURE 3: *In vitro* conformations of lysozyme determined from shape-reconstruction analysis of the SANS data in Figure 1. Best-fit structures are shown in blue, and consensus envelopes are shown in red. The crystal structure of lysozyme (PDB code 6LYZ, space-filling and ribbon) is shown for comparison with arrows pointing to the active-site cleft between the α and β domains.

between the α and β domains (*2*), the mechanism of BSA unfolding (*1*, *3*), and the ropelike structures of pre-amyloid oligomers (*4*).

As shown in Figure 3, SANS can determine the conformation of partially unfolded conformations unattainable with traditional crystallography. Thus, while at low azoTAB concentrations (3.6 mM under visible light and up to 12 mM under UV light) the SANS-based structures are similar to the crystal structure of pure lysozyme, the true utility of SANS is seen at elevated azoTAB concentrations were the degree, and location, of protein swelling can be determined. From examination of Figure 3, lysozyme is observed to swell primarily in the lower portion of the molecule away from the active site in the so-called hinge region, which gives rise to a progressively open active-site cleft. This unfolding mechanism is similar to previous SANS and FT-IR measurements at pH 7, which demonstrated that swelling induced by a similar azoTAB derivative was also in the hinge region and accompanied by a loss of α-helical content (*2*). The similarity in the unfolding mechanism observed in Figure 3 at pH 5 and in previous work at pH 7 illustrates the robust nature of shape-reconstruction of SANS data to examine the structure of partially unfolded proteins.

Note that the appearance of the swollen hinge regions in Figure 3 cannot be an artificial result of simple surfactant binding, and instead must be due to legitimate protein unfolding at this location. Surfactant binding to the protein can be separated into two possible mechanisms: single-molecule binding events or binding of surfactant aggregates (i.e., micelles). Binding of individual azoTAB molecules to lysozyme does of course occur, and as argued below is the likely mechanism by which the protein unfolds. Individual molecular binding would be expected to slightly increase the measured overall size of the protein through an effective increase in the molecular weight of the scattering species (protein plus bound surfactant). For example, at the surfactant concentration where lysozyme swelling is first observed in Figure 3 (8.5 mM azoTAB), comparing the protein (0.69 mM) and surfactant concentrations gives 12 surfactant molecules available for binding to the protein. Assuming complete surfactant binding with no surfactant free in solution (a conservative overestimation) and using the relationship $R_g \propto M_w^{0.369}$ for globular proteins (*48*), this would equate to at most an increase in the radius of gyration from 12.9 to 14.4 Å, much lower than the experimental value of 17.0 Å (see Table 1). Furthermore, the location of binding

of individual surfactant molecules would not typically be detected in the SANS measurements (except through the aforementioned global increase in the radius of gyration), which probe length scales ($L = 2\pi/Q$) of *ca.* 20−1250 Å, larger than molecular dimensions. Thus, the observed swollen hinge regions cannot be due to simple binding of individual surfactant molecules and, instead, must be due to either an unfolding of the protein at this location, or alternatively the binding of a surfactant aggregate/micelle (with dimension > 20 Å) at this location.

The phenomenon of surfactant aggregation onto a protein is commonly referred to as the "necklace-and-bead model", useful for proteins in the presence of high concentrations of sodium dodecyl sulfate (SDS) with SDS micelles (the "beads") aggregating along the unfolded protein chain (the "necklace") (*49*). In contrast, the SANS experiments in Figure 1 correspond to at most 5 to 26 surfactant molecules bound per protein, assuming complete binding. These values are much smaller than typical aggregation numbers of even a single micelle "bead", ranging from 40−100 SDS molecules per micelle (*50*, *51*), indicating the total amount of surfactant available for binding is likely not enough to correspond to a bound aggregate/micelle of sufficient size to be detected in the SANS measurements (i.e., >20 Å).

Nevertheless, a control experiment was performed at the protein contrast-matching point (60/40 H_2O/D_2O) (*52*) to render the protein "invisible" to the neutron beam, giving a SANS scattering intensity nearly identical to that of the solvent alone, with a difference on the order of $I \sim 10^{-3}$ cm^{-1}, i.e., within the experimental noise (compare to Figure 1). This conclusively demonstrates that azoTAB micellar aggregation on the protein is not contributing to an artificial increase in the scattering intensity. Thus, the swollen regions in Figure 3 must be due to protein unfolding, consistent with previously published FT-IR measurements that revealed significant changes in the secondary structure of lysozyme in the presence of azoTAB (*2*).

From these SANS-based *in vitro* conformations, the question remains as to what effect, if any, the increased exposure of the active-site cleft would have on lysozyme activity. Based on the conformations in Figure 3, however, any effect of azoTAB on lysozyme activity is expected be photoreversible since the *trans*, visible-light form of the surfactant induces a greater degree of active-site exposure compared to the *cis*, UV-light conformation.

Lysozyme Activity Determined by Ml-RBB. To determine the effect of surfactant and photoinitiated conformational changes on protein function, hydrolysis of dye-labeled *Micrococcus luteus* (Ml-RBB) with lysozyme was measured as a function of azoTAB concentration and light conditions, as shown in Figure 4a. At low azoTAB concentrations, lysozyme activity is *enhanced* with surfactant under both UV and visible light, while elevated azoTAB concentrations result in a maximum in the activity curves and eventual deactivation of the enzyme. Interestingly, both the onset of "superactivity" and enzyme deactivation are observed at lower azoTAB concentrations under visible compared to UV light.

While an enhancement of activity relative to the native state could be consistent with the increase of active-site exposure in the SANS-based *in vitro* structures above (discussed further below), the origin of the deactivation step

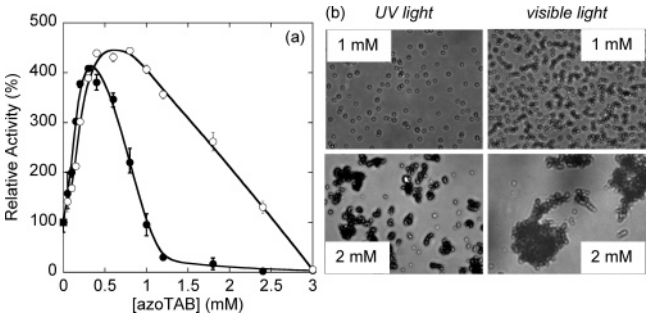

FIGURE 4: (a) Effect of azoTAB concentration on lysozyme activity against *Micrococcus luteus*-RBB under visible (●) and UV (○) illumination. [Lysozyme] = 0.002 mg/mL; [*Micrococcus luteus*-RBB] = 0.8 mg/mL. (b) Optical micrographs of *Micrococcus luteus*-RBB cells (0.8 mg/mL) as a function of azoTAB concentration and light conditions.

remains unclear. At least two possible factors could be responsible for this latter effect. First, azoTAB concentrations greater than 0.5 mM could induce complete protein denaturation as opposed to swelling in Figure 3, with the relatively hydrophobic *trans* form of the surfactant resulting in greater unfolding compared to the relatively hydrophilic *cis* isomer. Note that while 0.5 mM azoTAB is low compared to the surfactant concentrations in Figure 3, the significant difference in lysozyme concentrations required for the activity (0.002 mg/mL) and SANS (10 mg/mL) measurements does not allow ruling out this phenomenon.

Conversely, the decrease in activity at elevated azoTAB concentrations could result from surfactant interacting directly with the substrate, resulting in an effective loss of activity without changing the enzyme conformation. *M. luteus* is a Gram-positive bacterium with a negatively charged cell wall consisting of a rigid layer of highly cross-linked peptidoglycan embedded with teichuronic acids. At physiological pH, lysozyme exhibits a net positive charge (pI = 11.0), thus, the negative charge on the cell wall has been determined to be an important feature during hydrolysis (*37*, *53*). Thus, the presence of cationic azoTAB could neutralize the cell walls, leading to an effective decrease in enzyme reactivity. To examine this effect, optical micrographs of Ml-RBB cells were obtained under varying surfactant concentrations and light conditions, as shown in Figure 4b. At low azoTAB concentrations (<0.5 mM under visible [not shown] and 1 mM under UV light), the bacterial cells remain well dispersed in solution, indicating that much of the negative charge of the cells responsible for dispersion remains intact. With increased surfactant concentration, however, the *M. luteus* cells exhibit enhanced aggregation, becoming particularly pronounced beyond *ca.* 1 mM and 2 mM azoTAB under visible and UV light, respectively, consistent with regions of diminished activity in Figure 4a. Apparently, enhanced cell aggregation causes the accessibility of lysozyme to the peptidoglycin substrate to be substantially reduced, explaining the loss of activity observed above. The hydrophobic *trans* isomer results in a higher degree of cell aggregation compared to the *cis* isomer. Interestingly, cell aggregation and return to the well-dispersed state could be repeatedly and reversibly initiated with visible ↔ UV light cycles and the appropriate azoTAB concentration (not shown).

Lysozyme Activity Determined by Glycolchitin-RBB. Based on the above results, the standard Ml-RBB assay cannot

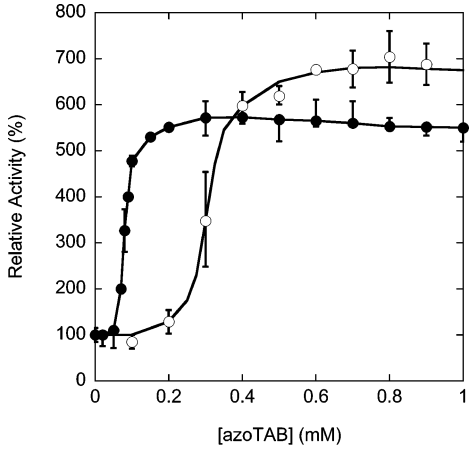

FIGURE 5: Lysozyme activity against glycolchitin-RBB as a function of azoTAB concentration under visible (●) and UV (○) illumination, respectively. [Lysozyme] = 0.002 mg/mL; [glycolchitin-RBB] = 1.5 mg/mL; pH 5.0; 37 °C.

properly assess the effect of azoTAB on lysozyme activity. Thus, a glycolchitin-RBB assay was used to minimize electrostatic interactions between the substrate and azoTAB. Glycolchitin is a neutral polymer composed of *N*-acetyl-D-glucosamine, and even when reacted with the anionic dye Remazol brilliant blue (degree of substitution ~ 2%) the net negative charge of glycolchitin-RBB is significantly lower than the *M. luteus* substrate. Lysozyme activity against glycolchitin-RBB as a function of azoTAB concentration and light conditions are shown in Figure 5. As was the case with the *M. luteus* substrate, enhanced activity over the native state is observed with increased azoTAB concentration. In contrast to Figure 4, however, the respective activities under visible and UV light level off at about 0.3 mM *trans* azoTAB and 0.6 mM *cis* azoTAB and remain essentially constant up to 12 mM azoTAB (data not shown). Thus, the decrease in activity at elevated azoTAB concentrations in Figure 4 does indeed appear to be an artifact of the cell aggregation due to neutralization.

With the effects of cell wall aggregation removed, 500−600% superactivity is observed with as little as 0.1 mM azoTAB under visible light and 600−700% superactivity occurs at ~0.3 mM surfactant under UV light. While a small degree of photocontrolled activity was observed with Ml-RBB at low surfactant concentrations ([azoTAB] < 0.3 mM), in Figure 5 without the depressing effect of cell aggregation the differences in activity between the visible and UV states are better resolved. Thus, it appears that at low surfactant concentrations lysozyme exhibits higher activity in the presence of the hydrophobic *trans* isomer compared to systems containing *cis* azoTAB as well as the native state. These results correlate with the shape-reconstruction analysis of the SANS data in Figure 3, which indicate that the *trans* form of azoTAB induces a higher degree of protein swelling than the hydrophilic *cis* form.

At relatively high azoTAB concentrations, however, lysozyme is seen to exhibit a slightly higher activity in the presence of *cis* versus *trans* azoTAB, related to two possible effects. First, even with the glycolchitin-RBB substrate chosen to minimize substrate−surfactant interactions, a small amount of residual interactions could account for the *trans* activity data being somewhat lower than the *cis* data at elevated surfactant concentrations. Second, the relatively hydrophobic *trans* isomer of azoTAB, being more prone to bind to lysozyme through nonspecific hydrophobic interactions, could potentially result in partial denaturation at the active size at elevated surfactant concentrations (as opposed to the specific swelling of the hinge region observed at relatively low surfactant concentrations), thus, leading to some degree of deactivation versus the *cis* state. Regardless, these are clearly only secondary effects, as lysozyme superactivty is observed to remain at the plateau values in Figure 5 to well beyond 12 mM azoTAB.

To determine enzyme kinetic parameters, initial velocity verses substrate concentration profiles and double-reciprocal Lineweaver−Burk plots of lysozyme against glycolchitin-RBB were generated, as shown in Figure 6. Interestingly, the initial-velocity profiles all go through a maximum in substrate concentration, suggesting eventual substrate inhibition of the enzyme. From the Lineweaver−Burk plots in Figure 6b, substrate inhibition is evident at low values of inverse substrate concentration; thus, the kinetic parameters in Table 2 were obtained using the linear portion of the data from a slope (K_M/V_m) and *x*-intercept ($-1/K_M$). Due to a very limited linear region for the *cis* azoTAB data (not shown), apparent kinetic parameters were only estimated for pure lysozyme and lysozyme in the presence of *trans* azoTAB. For native lysozyme activity against *M. luteus*, a similar substrate-inhibition effect has been observed, attributed to the strong electrostatic attraction between substrate and enzyme causing multiple attachments of substrates to the enzyme and hindering the substrate entering enzyme active site (*54*). However, the inhibition effect observed in Figure 6 is less likely to be a result of electrostatic attraction considering the low charge of glycolchitin-RBB compared to *M. luteus*. Thus, the major inhibition effect may be the competing transglycolsylation reaction (*55*). As mentioned above, the active site of lysozyme is divided into six subsites *A*−*F*. The scissile bond locates between subsites *D* and *E*, with cleavage of the $\beta(1\rightarrow4)$ linkage of the polysaccharide leading to the formation of a positively charged oxocarbenium intermediate bound to site *A* through *D* and stabilized by Asp52. During the normal reaction pathway, a nucleophilic water molecule hydrolyzes this intermediate, forming a reduced-sugar product that is released from the active site. However, if a second substrate occupies the vacant sites *E* and *F* prior to hydrolysis, a $\beta(1\rightarrow4)$ linkage between the intermediate and this second substrate can occur, resulting in transglycosylation (*19*−*21*). Thus, elevated substrate concentrations can increase the occurrence of the competing transglycosylation reaction, the likely origin of the substrate inhibition observed in Figure 6.

As shown in Table 2, both the Michaelis constant K_M and the maximum velocity V_m increase in the presence of 0.2 mM *trans* azoTAB. Assuming that the rate-limiting step is product formation, K_M represents the dissociation constant between enzyme and substrate; thus, the increase of K_M suggests a decrease in substrate binding affinity toward the slightly unfolded form of lysozyme in the presence of *trans* azoTAB compared to the native state. In contrast, the 8-fold increase in the maximum velocity V_m, which can be related to an increase in the enzyme turnover number k_{cat} through the equation $k_{cat} = V_m/[E]_0$, suggests that the swollen structures of lysozyme in the presence of *trans* azoTAB have the effect of increasing the overall reaction rate. Recalling

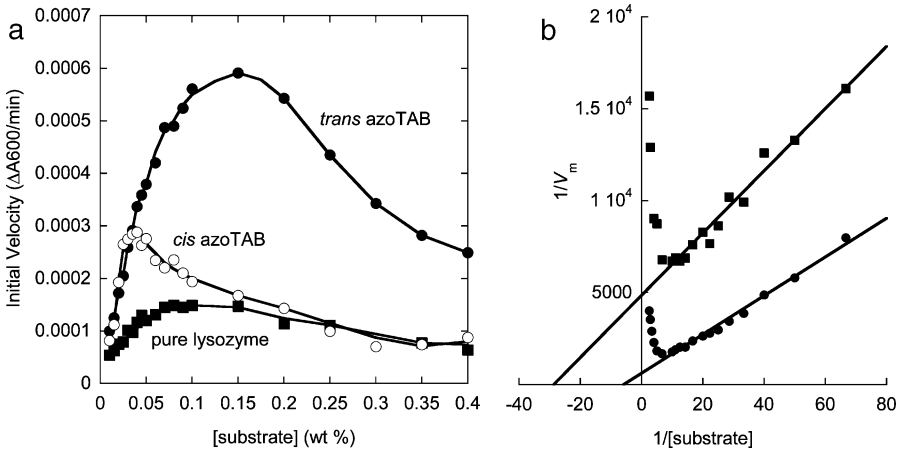

FIGURE 6: (a) Initial velocity profile of lysozyme against glycolchitin-RBB without (■) and with 0.02 mM *trans* azoTAB (●) and *cis* azoTAB (○). (b) Linweaver-Burk plot of native lysozyme (■) and lysozyme with 0.2 mM *trans* azoTAB (●). [lysozyme] = 0.002 mg/mL; pH 5.0; 37 °C.

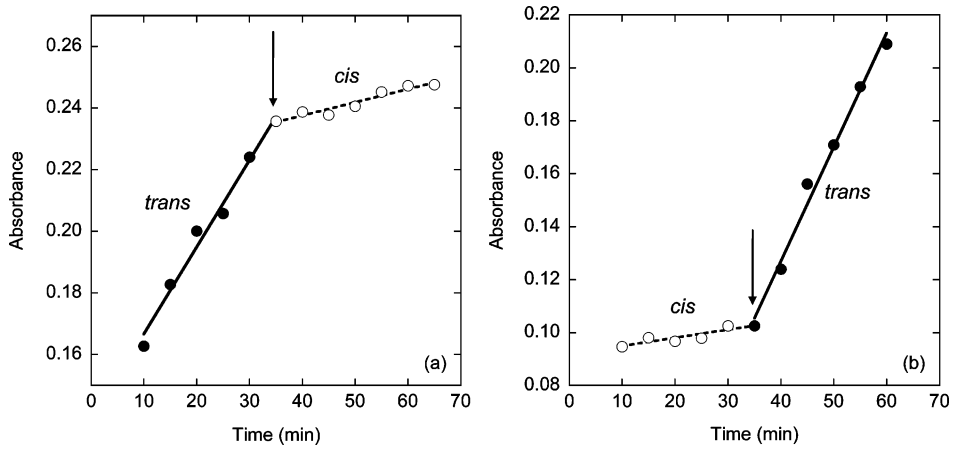

FIGURE 7: Photoregulation of lysozyme activity against glycolchitin-RBB. (a) Reaction initiated with *trans* azoTAB (—), followed by UV illumination to photoisomerize azoTAB to the *cis* state (- - -). (b) Reaction initiated with *cis* azoTAB (- - -), followed by visible illumination to photoisomerize azoTAB to the *trans* state (—). [lysozyme] = 0.002 mg/mL, [glycolchitin-RBB] = 1.5 mg/mL, [azoTAB] = 0.2 mM, pH 5.0; 37 °C. Arrows indicate points at which UV or visible illumination was initiated.

Table 2: Effect of azoTAB on the Kinetic Parameters of Lysozyme[a]

azoTAB (mM)	K_M (mg/mL)	$10^4 \times V_m$ (A_{600}/min)
0	0.34	2.06
0.2 (*trans*)	1.72	16.3

[a] [Lysozyme] = 0.002 mg/mL, pH 5.0.

the SANS-based *in vitro* structures can provide insight to these two effects. With the net increase in the separation distance of the two domains, likely a result of enhanced domain motions in the presence of *trans* azoTAB, the substrate binding affinity has been reduced due to a slight perturbation of the active site, yet the reaction is enhanced due to an increase in flexibility of the enzyme. The later occurrence of substrate inhibition with *trans* azoTAB may also be a result of enhanced flexibility favoring hydrolysis (increase in V_m) over transglycosylation (decrease in substrate binding affinity).

In order to form the enzyme−substrate complex, it has been reported that the active-site cleft of lysozyme has to first open (to allow the substrate to enter the active site) and then close (to return the enzyme to a state similar to the native conformation) through hinge-bending motions of the α and β domains (*56*−*62*). Thus, it may be expected that domain motions play an important role in the enzyme catalytic process. Indeed, a number of studies support this relationship between conformational flexibility and enzyme activity (*63*−*66*), with increases in flexibility and internal fluctuation leading to enhanced enzyme activity (*22*, *23*, *67*−*69*). For the specific case of lysozyme, a mutant with residues Arg14 and His15 deleted has exhibited increased internal motions upon inhibitor binding and higher activity against glycholchitin comparing to the wild-type enzyme, despite the fact that both of these residues are distal the active-site cleft (*22*, *23*). Similarly, replacing the bulky tryptophan residue at subsite B of the active site with smaller tyrosine or phenylalanine residues gave looser binding of substrates yet enhanced activity by up to 200% (*70*, *71*). Conversely, when residues Met12 (α-helix) and Leu56 (β-sheet), which face each other across the cavity of the hydrophobic core in the α domain, were replaced with more hydrophobic residues, the mutant exhibited enhanced stability and rigidity and a reduction in activity, possibly due to restricted internal motions (*68*).

The rates of enzymatic reactions are controlled by the height of the activation energy barrier, or equivalently the probability of sampling transition-state conformations. Thus, to induce superactivity requires that enzyme flexibility be increased in such a way that these transition-state structures

are preferentially sampled, with flexibility promoting conformational changes along the reaction pathway (*8*, *12*−*14*). With this view, the increase in activity observed under visible light could be a result of the higher degree of swelling localized near the hinge region, which would be expected to lead to enhanced hinge-bending motions and a net increase in the separation distance of the α and *β* domains. At the ensemble level as in Figure 3, this is manifested by an overall broadening of the active-site cleft, with the SANS structures representing the *z*-average of all conformations in solution (*4*), analogous to regions with high-temperature factors (*B* factors) in X-ray crystallographic structures that are often associated with regions undergoing large thermal motions. Thus, azoTAB appears to induce superactivity in lysozyme by binding at a location removed from the active site and resulting in a more flexible enzyme undergoing fluctuating conformational changes.

In Situ Photocontrol of Enzyme Activity. One potential application of the photoresponsive azoTAB surfactant is to act as a photoregulator in biocatalytic systems, where simple light illumination can be used for *in situ* control of enzyme activity. Figure 7 demonstrates this photoregulation of lysozyme activity against glycolchitin-RBB. In Figure 7a the reaction begins with 0.2 mM *trans* azoTAB (∼550% superactivity from Figure 5), followed by UV illumination to convert azoTAB to the *cis* state, immediately leading to a decrease in reaction rate (activity ∼120%), a result of enhanced protein swelling under visible versus UV light. While similar photoswitching of biocatalytic activity has been obtained through covalent attachment of photoresponsive groups to an enzyme (*72*−*74*), this enzyme modification process is relatively complex and time-consuming compared to simple mixing of enzymes with the azoTAB surfactant. Furthermore, with covalent linkages enzyme activity is typically decreased slightly compared to the native state even in the "on" state (*72*−*74*). In contrast, azoTAB offers a unique method to induce superactivity through interacting with hydrophobic, often α-helical regions of the protein removed from the active site.

ACKNOWLEDGMENT

We thank W. T. Heller for graciously supplying the GA_STRUCT program. We acknowledge the support of the National Institute of Standards and Technology, U.S. Department of Commerce, in providing the neutron research facilities used in this work.

REFERENCES

1. Lee, C. T., Jr., Smith, K. A., and Hatton, T. A. (2005) *Biochemistry 44*, 524−536.
2. Hamill, A. C., Wang, S.-C., and Lee, C. T., Jr. (2005) *Biochemistry 44*, 15139−15149.
3. Wang, S.-C., and Lee, C. T., Jr. (2006) *J. Phys. Chem. B 110*, 16117−16123.
4. Hamill, A., Wang, S.-C., and Lee, C. T., Jr. (2007) *Biochemistry 46*, 7694−7705.
5. Eastoe, J., and Vesperinas, A. (2005) *Soft Matter 1*, 338−347.
6. Cannon, W. R., Singleton, S. F., and Benkovic, S. J. (1996) *Nat. Struct. Biol. 3*, 821−833.
7. Bruice, T. C., and Benkovic, S. J. (2000) *Biochemistry 39*, 6267−6274.
8. Benkovic, S. J., and Hammes-Schiffer, S. (2003) *Science 301*, 1196−1202.
9. Zhang, X., and Houk, K. N. (2005) *Acc. Chem. Res. 38*, 379−385.
10. Olsson, M. H. M., Parson, W. W., and Warshel, A. (2006) *Chem. Rev. 106*, 1737−1756.
11. Benkovic, S. J., and Hammes-Schiffer, S. (2006) *Science 312*, 208−209.
12. Schramm, V. L. (2005) *Curr. Opin. Struct. Biol. 15*, 604−613.
13. Hammes-Schiffer, S. (2002) *Biochemistry 41*, 13335−13343.
14. Vendruscolo, M., and Dobson, C. M. (2006) *Science 313*, 1586−1587.
15. Tousignant, A., and Pelletier, J. N. (2004) *Chem. Biol. 11*, 1037−1042.
16. Hammes-Schiffer, S., and Benkovic, S. J. (2006) *Annu. Rev. Biochem. 75*, 519−541.
17. Cameron, C. E., and Benkovic, S. J. (1997) *Biochemistry 36*, 15792−15800.
18. Warshel, A., and Levitt, M. (1976) *J. Mol. Biol. 103*, 227−249.
19. Imoto, T., Johnson, L. N., North, A. C. T., Phillips, D. C., and Rupley, J. A. (1972) *The Enzymes*, 3rd ed., Vol. 7, pp 665−868, Academic, New York.
20. Johnson, L. N., and Phillips, D. C. (1965) *Nature 206*, 761−763.
21. Fukamizo, T., Minematsu, T., Yanase, Y., Hayashi, K., and Goto, S. (1986) *Arch. Biochem. Biophys. 250*, 312−321.
22. Mine, S., Tate, S., Ueda, T., Kainosho, M., and Imoto, T. (1999) *J. Mol. Biol. 286*, 1547−1565.
23. Imoto, T., Ueda, T., Tamura, T., Isakari, Y., Abe, Y., Inoue, M., Miki, T., Kawano, K., and Yamada, H. (1994) *Protein Eng. 7*, 743−748.
24. Hayashi, K., Kugimiya, M., Imoto, T., Funatsu, M., and Bigelow, C. C. (1968) *Biochemistry 7*, 1467−1472.
25. Hayashi, K., Kugimiya, M., Imoto, T., Funatsu, M., and Bigelow, C. C. (1968) *Biochemistry 7*, 1461−1466.
26. Jones, M. N., Prieto, G., Rio, J. M. d., and Sarmiento, F. (1995) *J. Chem. Soc., Faraday Trans.* 2805−2809.
27. Liu, H., Yang, W., and Chen, J. (1998) *Biochem. Eng. J. 2*, 187−196.
28. Svergun, D. I., Petoukhov, M. V., and Koch, M. H. (2001) *Biophys. J. 80*, 2946−2953.
29. Heller, W. T., Krueger, J. K., and Trewhella, J. (2003) *Biochemistry 42*, 10579−10588.
30. Shang, T., Smith, K. A., and Hatton, T. A. (2003) *Langmuir 19*, 10764−10773.
31. Hayashita, T., Kurosawas, T., Miyata, T., Tanaka, K., and Igawa, M. (1994) *Colloid Polym. Sci. 272*, 1611−1619.
32. Durchschlag, H., Hefferle, T., and Zipper, P. (2003) *Radiat. Phys. Chem. 67*, 479−486.
33. Durchschlag, H., Fochler, C., Feser, B., Hausmann, S., Seroneit, T., Swientek, M., Swoboda, E., Winklmair, A., Wlcek, C., and Zipper, P. (1996) *Radiat. Phys. Chem. 47*, 501−505.
34. Shugar, D. (1952) *Biochim. Biophys. Acta 8*, 302−309.
35. Le Ny, A.-L. M., and Lee, C. T., Jr. (2006) *J. Am. Chem. Soc. 128*, 6400−6408.
36. Ito, Y., Yamada, H., and Imoto, T. (1992) *Chem. Pharm. Bull. 40*, 1523−1526.
37. Richards, P. G., Walton, D. J., and Heptinstall, J. (1996) *Biochem. J. 315*, 473−479.
38. Wirth, S. J., and Wolf, G. A. (1990) *J. Microbiol. Methods 12*, 197−205.
39. Yamasaki, N., Tsujita, T., and Takakuwa, M. (1973) *Agric. Biol. Chem. 37*, 1507−1508.
40. Eisenthal, R., Danson, M. J., and Editors (1992) *Enzyme Assays: A Practical Approach*, Oxford University Press, New York.
41. Sadana, A. (1991) *Biocatalysis: Fundamentals of Enzyme Deactivation Kinetics*, Prentice Hall, Inc., Englewood Cliffs, NJ.
42. Glinka, C. J., Barker, J. G., Hammouda, B., Krueger, S., Moyer, J. J., and Orts, W. J. (1998) *J. Appl. Crystallogr. 31*, 430−445.
43. Stenstam, A., Montalvo, G., Grillo, I., and Gradzielski, M. (2003) *J. Phys. Chem. B 107*, 12331−12338.
44. Stuhrmann, H. B., and Fuess, H. (1976) *Acta Crystallogr., Sect. A: Cryst. Phys., Diffr., Theor. Gen. Crystallogr. A32*, Part 1, 67−74.
45. Kamatari, Y. O., Konno, T., Kataoka, M., and Akasaka, K. (1998) *Protein Sci. 7*, 681−688.
46. Chen, L., Hodgson, K. O., and Doniach, S. (1996) *J. Mol. Biol. 261*, 658−672.
47. Svergun, D. I., and Koch, M. H. J. (2003) *Rep. Prog. Phys. 66*, 1735−1782.
48. Uversky, V. N. (1993) *Biochemistry 32*, 13288−13298.
49. Chen, S. H., and Teixeira, J. (1986) *Phys. Rev. Lett. 57*, 2583−2586.

50. Ibel, K., May, R. P., Kirschner, K., Szadkowski, H., Mascher, E., and Lundahl, P. (1990) *Eur. J. Biochem. 190*, 311−318.
51. Turro, N. J., Lei, X.-G., Ananthapadmanabhan, K. P., and Aronson, M. (1995) *Langmuir 11*, 2525−2533.
52. Bendedouch, D., and Chen, S. H. (1983) *J. Phys. Chem. 87*, 1473−1477.
53. Tanford, C., and Wager, M. L. (1954) *J. Am. Chem. Soc. 76*, 3331−3336.
54. Verhamme, I. M. A., Van Dedem, G. W. K., and Lauwers, A. R. (1988) *Eur. J. Biochem. 172*, 615−620.
55. Banerjee, S. K., Kregar, I., Turk, V., and Rupley, J. A. (1973) *J. Biol. Chem. 248*, 4786−4792.
56. Zhang, X.-j., Wozniak, J. A., and Matthews, B. W. (1995) *J. Mol. Biol. 250*, 527−552.
57. Kuroki, R., Weaver, L. H., and Matthews, B. W. (1993) *Science 262*, 2030−2033.
58. Goto, N. K., Skrynnikov, N. R., Dahlquist, F. W., and Kay, L. E. (2001) *J. Mol. Biol. 308*, 745−764.
59. Chen, Y., Hu, D., Vorpagel, E. R., and Lu, H. P. (2003) *J. Phys. Chem. B 107*, 7947−7956.
60. Wagner, G., Hyberts, S. G., and Havel, T. F. (1992) *Annu. Rev. Biophys. Biomol. Struct. 21*, 167−198.
61. Faber, H. R., and Matthews, B. W. (1990) *Nature 348*, 263−266.
62. Matthews, B. W. (1995) *Adv. Protein Chem. 46*, 249−278.
63. Poole, P. L., and Finney, J. L. (1983) *Int. J. Biol. Macromol. 5*, 308−310.
64. Gross, M., Auerbach, G., and Jaenicke, R. (1993) *FEBS Lett. 321*, 256−260.
65. Roh, J. H., Curtis, J. E., Azzam, S., Novikov, V. N., Peral, I., Chowdhuri, Z., Gregory, R. B., and Sokolov, A. P. (2006) *Biophys. J. 91*, 2573−2588.
66. Zavodszky, P., Kardos, J., Svingor, A., and Petsko, G. A. (1998) *Proc. Natl. Acad. Sci. U.S.A. 95*, 7406−7411.
67. Daniel, R. M., Dunn, R. V., Finney, J. L., and Smith, J. C. (2003) *Annu. Rev. Biophys. Biomol. Struct. 32*, 69−92.
68. Ohmura, T., Ueda, T., Ootsuka, K., Saito, M., and Imoto, T. (2001) *Protein Sci. 10*, 313−320.
69. Yoshida, Y., Ohkuri, T., Kino, S., Ueda, T., and Imoto, T. (2005) *Cell. Mol. Life Sci. 62*, 1047−1055.
70. Kumagai, I., and Miura, K. (1989) *J. Biochem. (Tokyo, Japan) 105*, 946−948.
71. Maenaka, K., Matsushima, M., Song, H., Sunada, F., Watanabe, K., and Kumagai, I. (1995) *J. Mol. Biol. 247*, 281−293.
72. Inada, T., Terabayashi, T., Yamaguchi, Y., Kato, K., and Kikuchi, K. (2005) *J. Photochem. Photobiol., A: Chem. 175*, 100−107.
73. Willner, I., Rubin, S., and Riklin, A. (1991) *J. Am. Chem. Soc. 113*, 3321−3325.
74. Willner, I., and Rubin, S. (1993) *React. Polym. 21*, 177−186.

BI701073D